Journal Pre-proofs

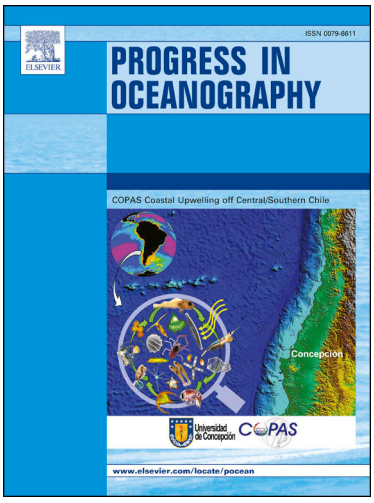

Three-dimensional cross-shelf zooplankton distributions off the Central Oregon Coast during anomalous oceanographic conditions

Christian Briseño-Avena, Moritz S. Schmid, Kelsey Swieca, Su Sponaugle, Richard D. Brodeur, Robert K. Cowen

PII: S0079-6611(20)30175-0
DOI: https://doi.org/10.1016/j.pocean.2020.102436
Reference: PROOCE 102436

To appear in: *Progress in Oceanography*

Received Date: 21 May 2019
Revised Date: 1 September 2020
Accepted Date: 2 September 2020

Please cite this article as: Briseño-Avena, C., Schmid, M.S., Swieca, K., Sponaugle, S., Brodeur, R.D., Cowen, R.K., Three-dimensional cross-shelf zooplankton distributions off the Central Oregon Coast during anomalous oceanographic conditions, *Progress in Oceanography* (2020), doi: https://doi.org/10.1016/j.pocean.2020.102436

Three-dimensional cross-shelf zooplankton distributions off the Central Oregon Coast during anomalous oceanographic conditions

Christian Briseño-Avena*[1,4], Moritz S. Schmid[1], Kelsey Swieca[1,2], Su Sponaugle[1,2], Richard D. Brodeur[3], Robert K. Cowen[1]

[1] Hatfield Marine Science Center, Oregon State University, Newport, OR 97365, USA

[2]Department of Integrative Biology, Hatfield Marine Science Center, Oregon State University, Newport, OR 97365, USA

[3]National Oceanic and Atmospheric Administration, Northwest Fisheries Science Center, Newport, Oregon 97365, USA

[4]Department of Environmental and Ocean Sciences, University of San Diego, San Diego, CA 92110, USA

*Corresponding author: Christian Briseño-Avena (cbriseno@ucsd.edu)

Abstract

The Northern California Current (NCC) is a complex, dynamic system experiencing distinctly different levels of upwelling and downwelling, ranging from intermittent upwelling in summer to downwelling in winter. In recent years, warm water anomalies along the Oregon coast have had significant effects on coastal plankton assemblages. To resolve some of the fine-scale responses to these conditions, we used a towed, undulating underwater imaging system to investigate fine-scale (1m vertical) zoo- and ichthyoplankton distributions along a 57-km section parallel to the Newport Hydrographic Line encompassing the shelf, shelf break, and slope off the central coast of Oregon. A sparse Convolutional Neural Network was used to automate the identification of 52 million plankton images of 64 plankton taxa, ranging from protists to copepods, larval fishes, and gelatinous organisms. Taxa distributions were interpolated over the whole transect, providing unprecedented insight into their horizontal and vertical distributions and revealing seven broad patterns of distribution. Additional fine-scale distribution data enable examination of some of the physical and biological processes underlying these fine-scale distribution patterns, building upon the historical time series data that exists for this region and advancing our knowledge of planktonic processes in this productive region of the NCC.

1. Introduction

The northern California Current (NCC) is a dynamic, highly productive oceanographic region within the broader California Current Large Marine Ecosystem (CCLME). It supports several robust fisheries, including Dungeness crab, pink shrimp, salmon, and albacore tuna, and has received significant scientific attention related to fisheries, climate, and ocean acidification (e.g., Shanks and Roegner, 2007, Childers et al. 2011, Phillips et al. 2014). Research on key fisheries species in the region has been instrumental in understanding the effects of regional to large-scale phenomena, such as the Pacific Decadal Oscillation (PDO) and El Niño, on zooplankton (Peterson & Keister, 2003, Keister & Peterson, 2003, Keister et al. 2011) and fish larvae (Brodeur et al. 2008, Auth et al. 2011). One consistent data stream within this system is the Newport Hydrographic Line (NH-Line) time series, which has been sampled regularly since 1961 (Peterson and Miller, 1975). More recently, the biological effects of the prolonged marine heat wave, informally referred to as “the Blob” (Bond et al. 2015), that affected the Oregon coast (USA) from 2014 to 2016 have been examined (Peterson et al. 2017, Auth et al. 2018, Brodeur et al. 2019), capitalizing on continued sampling on or near the NH-Line. The “Blob” brought an abrupt temperature increase to the central Oregon coast, with a reported +4.5^{o}C anomaly along the NH-Line (Peterson et al. 2017). The magnitude and duration of this warm event ranks among the most extreme marine heatwaves ever recorded (Hobday et al. 2018). During this anomalously warm period, higher biomasses of warm-water copepod species occurred on the NH-Line, an atypical observation for the region (Peterson et al. 2017). Furthermore, this marine heat wave had positive effects on gelatinous macrozooplankton, whose concentrations dramatically increased during 2016 relative to more normal years while other groups, such as crustaceans and teleosts showed a decrease in certain areas off the Oregon coast (Brodeur et al. 2019).

Most biological oceanographic work in the NCC has used plankton nets and trawl surveys to focus on crustacean zooplankton, particularly copepods and euphausiids (Peterson et al. 2002, Keister and Peterson, 2003, Peterson et al. 2017), ichthyoplankton (Brodeur et al. 2008, Auth et al. 2011, 2018), and more recently, macrozooplanktonic gelatinous organisms (Peterson et al. 2017, Brodeur et al. 2019). While these efforts have substantially advanced our understanding of this biologically-active region, the fine scale spatial and vertical distributions of these organisms and planktonic food web dynamics are poorly resolved (Francis et al. 2012). These limitations are further exacerbated by the need to understand the full range of biological responses to the variety of environmental perturbations impacting the NCC, including the warm Blob, El Niño and PDO oscillations, as well as hypoxia and ocean acidification. These knowledge gaps stem, in part, from sampling resolution limitations imposed by traditional

plankton sampling techniques, for instance, the coarse horizontal and vertical resolutions obtained by sampling with nets (Wiebe and Benfield, 2003; Cowen and Guigand, 2008; Richardson et al. 2009, Lombard et al. 2019). Net-based sampling typically necessitates the integration of large horizontal and vertical distances (and by extension, volume) and are thus inadequate to resolve the fine-scale distributions affecting predator-prey interactions or the biophysical factors influencing organisms at ecologically-significant scales. Furthermore, since most zoo- and ichthyoplankton sampling is conducted with nets, there is often a mismatch between these coarse resolution samples and the fine spatial and temporal resolution at which physical properties of seawater can be sampled (Cowen and Guigand, 2008). It is often at these finer scales that biophysical interactions are determined (Prairie et al. 2012, Schmid and Fortier 2019).

Finer-scale data can be collected on the scale of the individual through to sub-mesoscales (Luo et al. 2014, Schmid et al. 2018) using underwater imaging that can resolve not only the distributions of larval fishes, but also that of their patchy prey and predator fields. Several imaging systems are in existence today (e.g., Video Plankton Recorder (VPR), Davis et al. 2005; In Situ Ichthyoplankton Imaging System (ISIIS), Cowen and Guigand, 2008; Underwater Vision Profiler 5 (UVP5), Picheral et al. 2010; Lightframe On-sight Keyspecies Investigation (LOKI), Schmid et al. 2016), but their early usage has been limited, in part due to system costs and image analysis challenges associated with millions to billions of images.

Here we report the fine-scale, cross-shelf plankton distribution patterns (seascapes) and physical-biological interactions along a cross-shelf section immediately south of the NH-Line off the Oregon coast with a combined approach of *in situ* underwater imager and the automated identification of plankton on images using deep learning methods (Robinson et al. 2017, Luo et al. 2018). Our goal was to illustrate how fine-scale (down to 100 m deep), and cross-shelf plankton distributions, combined with associated environmental variables, can inform our understanding of system-wide processes. A second goal is to provide information on a wider range of organisms (e.g., protists, *Oithona* sp., hydromedusae, siphonophores) for inclusion into the valuable historic time-series data that exist for the area. Finally, our *in situ* study coincided with the end of “the Blob” (Summer 2016) and was coupled with concurrent traditional net sampling (Brodeur et al. 2019), providing an ideal opportunity to examine the knowledge gaps that can be filled with such high resolution underwater imaging.

2. Methods

2.1. *Study area*

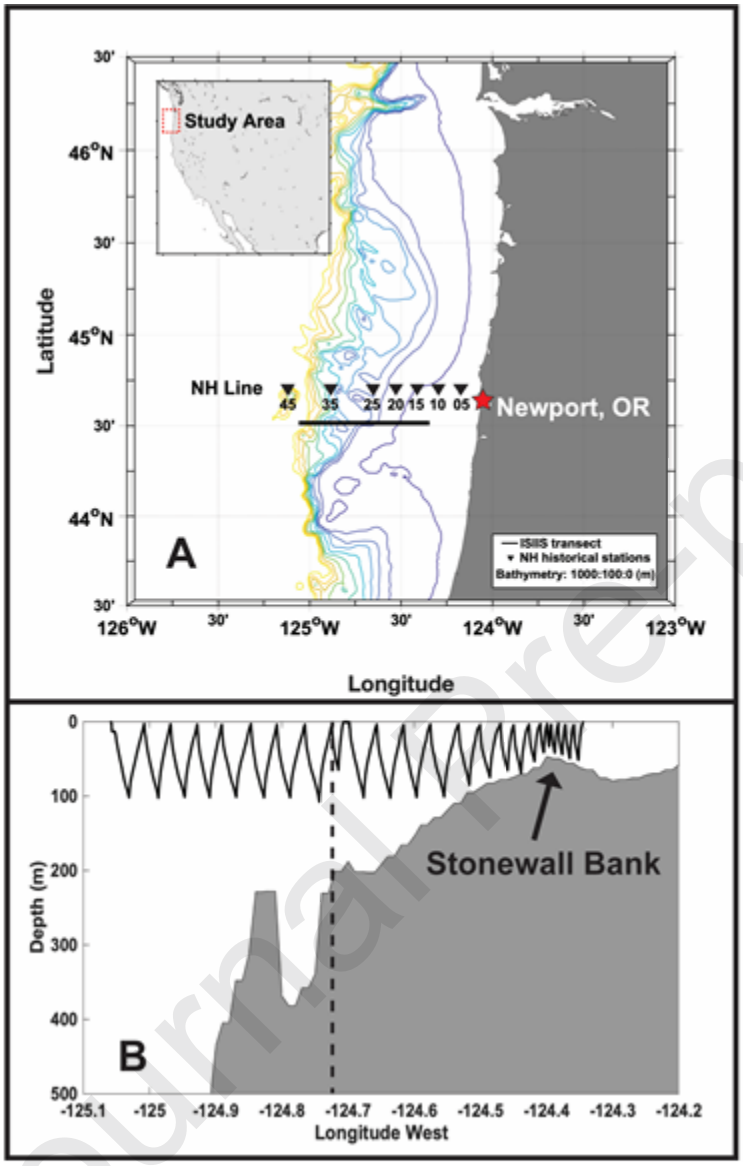

Fig. 1. A. Study area showing the ISIIS tow transect (solid horizontal black line) along the NH-ISIIS line and the current NH-Line (triangles). Isobaths were drawn from 1000 m to 0 m at 100 m increments. **B.** ISIIS towpath plotted over bathymetric features. Vertical dashed line indicates the approximate location of the shelf break (200 m isobath).

Located off Newport, Oregon (Fig 1A), the nominal Newport Hydrographic Line (NH-Line) time series sampling started in 1996 (Peterson et al. 2014) with the primary goal of understanding the biophysical drivers of the recruitment of commercially important fish species in the NCC, though sampling along this line has existed since 1961 (Peterson and Miller, 1975). The data presented here were collected aboard the NOAA Fisheries Research Vessel *Bell M. Shimada*, as part of NOAA Northwest Fisheries Science Center's 2006 Pre-Recruit Survey (PRS). While the NH-Line stations are centered at 44°39'N (triangles in **Fig. 1A**), the PRS program has zonal cross-shelf transects regularly spaced every 0.5 degree of latitude from the Oregon-California to the Oregon-Washington (USA) borders. Since the transect for this project (solid line in **Fig. 1A**) is 0.15° south of the NH-Line, we refer to our sampling line as Newport Hydrography-ISIIS (NH-ISIIS). The data presented here were collected during the daylight hours (0853-1445) on June 25, 2016. Unfortunately, no nighttime deployments were conducted during this research cruise.

2.2. *The In Situ Ichthyoplankton Imaging System (ISIIS)*

ISIIS (Cowen and Guigand, 2008) is a towed shadowgraph imager that utilizes a high resolution line-scan camera (68 μm pixel) to image a large volume of water (150-185 L s^{-1}) to allow both common and rare mesozooplankters, including larval fishes, to be imaged (Cowen et al. 2013). ISIIS' large imaging frame, with 13 x 13-cm field of view and 50 cm depth of field allows for the undisturbed imaging of fragile gelatinous zooplankton (McClatchie et al. 2012, Luo et al. 2014, 2018) and evasive, highly motile taxa like euphausiids and fish larvae. Data are sent to a top-side computer using a fiber optic cable where imagery data are time-stamped and stored. ISIIS is equipped with a CTD (Sea-Bird SBE 49 FastCAT), as well as environmental sensors that record dissolved oxygen (Sea-Bird 43), Chl-*a* fluorescence (Wet Labs FLRT), and photosynthetically active radiation (PAR; Biospherical QCP-2300). During this study, ISIIS was towed during daylight hours in an undulating fashion from the surface to 100 m depth or to within a few meters (mean 8.9 ± 3.7 m SD, depending on sea conditions) of the seafloor (**Fig. 1B**) at 2.5 m s^{-1} (speed through the water). Sampling was continuous along the full 57 km NH-ISIIS transect, and resulted in 24 full undulations, and a total of 345,290 image frames.

2.3 *In Situ Image Processing and Automated Classification Pipeline*

The collected imagery (**Fig. 2**) was used in the training and testing of a sparse Convolutional Neural Network (sCNN**)** for the automated identification of taxa following standard

protocols established in Luo et al., (2018). sCNNs (LeCun al. 2015) are the state of the art for automated identification of plankton specimens from underwater images (Dieleman et al. 2016, Luo et al. 2018). sCNNs identify which characteristics within images are best for classification, and exploit the fact that images can be analyzed in a hierarchical fashion, from smaller features to larger features (LeCun al. 2015). Below is a brief description of the methods and pipeline pertaining to this dataset (see Luo et al. 2018 for more details).

Fig. 2. Diversity of planktonic organisms imaged with ISIIS on June 25, 2016 along the NH-ISIIS transect. These are representative taxa of some of the categories used in the training library for the sCNN. Scale bars are given for each individual taxon.

2.3.1. *Image Processing*

The video data (avi file stacks with fixed number of frames) obtained by ISIIS were de-stacked into single frames (13 x 13 cm), flat-fielded (background subtraction using a k-harmonic means clustering algorithm) and then regions of interest (ROI; i.e., a single plankton specimen) were detected and segmented (or extracted). These ROIs (hereafter referred to as vignettes) were then saved as jpg files and tarballed (a file compression method; tar.gz file extension) per avi stack in preparation for the automated classification pipeline. The number of vignettes differed between tarballed stacks, depending on how many vignettes were detected by the segmentation algorithm.

2.3.2 *Training Library using Shimada ISIIS imagery on the sparse Convolutional Neural Network (sCNN)*

The training library (TL) consisted of 161 different categories of plankton, particles, and noise artifacts (**Fig. 2**, **Supplementary Table 1**). The vignettes for the TL were selected randomly from the entire imagery collection, and manually sorted into each of the 161 categories (referred to as classes). A total of 51,870 vignettes were used to train the library, accurately representing the diversity of organisms present in the region at different taxonomic levels. Organisms in the TL were classified to the lowest possible taxonomic level.

Due to the disproportionately high number of common organisms and particles (e.g. marine snow) in the original data, and fewer rare organisms, the number of training vignettes for most classes ranged between several hundreds to thousands of vignettes, while for rare taxa the number of vignettes ranged from 20-100. This did not present an issue as sCNNs have the ability to augment data (Luo et al. 2018). The sCNN used was *SparseConvNets with Fractional Max-Pooling* (Graham et al. 2015), following closely the methodology developed in Luo et al. (2018). The sCNN was trained until an error rate of ≤ 5% was attained at 400 epochs.

A total of 15,791 vignettes were randomly extracted from the same NH-ISIIS transect dataset and manually identified to generate an unbiased test set. The same vignettes were then identified using the trained sCNN, generating a probability that each vignette belonged to any one of the 161 classes (probabilities per vignette sum to one), where the class with the highest probability is selected as the predicted automated identification. This set was then used to estimate the Filtering Thresholds (FT) applied to each class before merging into their final groups.

2.3.3. *Filter-Thresholding*

To consolidate the different classes pertaining to a single taxon (e.g., Chaetognath curve, Chaetognath head, Chaetognath "s" shape, Chaetognath straight, and Chaetognath tail, are different shape classes for the taxon "Chaetognath"), the 161 original classes were mapped onto 72 final groups (**Supplementary Table 2**). Given that each class has a different classification performance, we applied FTs to exclude low-probability data. Removal of these "low-confidence images" still allows for the prediction of true spatial distributions (Faillettaz et al. 2016).

The FTs were estimated using the results from the independent test. The approach uses a LOESS model to determine at which probability threshold a cutoff should be made (at the original class level) to reach 90% classification precision at the broader group level. This is achieved by iteratively removing images of a class below a certain threshold and recalculating classifier precision (see Luo et al. (2018) and **Supplementary Table 1** for the applied thresholds). Vignettes with a maximum assigned probability less than or equal to the determined thresholds were re-classified as unknown.

2.3.4. *Performance of the sCNN*

To evaluate the final classification pipeline performance, we used confusion matrix analyses (Hu and Davis, 2006, Tharwat, 2018). A confusion matrix analysis is a powerful tool to determine how good or bad a prediction model performs. To carry out this exercise, a subset of images classified by the model need to be manually corroborated. For this work, we randomly generated a set of 86,681 vignettes from all final groups. These images were manually identified independently by three human experts and compared against their automated predicted classifications from the sCNN. A third pass was then made by one of the three human experts to correct for additional mistakes or inconsistencies between experts. We then estimated several metrics to reveal how the classifier performed for each taxon. These metrics (rates) are based on the number of true positive counts (TP), false positive counts (FP) and false negatives counts (FN) for each taxon in this data subset. Using these counts, we can determine precision rates for each taxon (P_{taxon}) and using:

$$P_{taxon} = TP / (TP + FP) \qquad \text{Eq. (1)}$$

And recall rates for each taxon calculated using:

$R_{taxon} = TP / (TP + FN)$ Eq. (2)

Finally, a related measure of overall performance of the classifier is measured by taking the first harmonic mean of the precision and recall for each taxon. This is referred to as Fscore and is calculated as:

$Fscore_{taxon} = 2*P_{taxon}*R_{taxon} / (P_{taxon} + R_{taxon})$ Eq. (3)

In each case, a higher value is indicative of a better classifier performance for a given group or taxon. These rates can be used together, or separately, to evaluate the performance of the classifier as a whole or for each class (taxon). While precision can be interpreted as how many of the selected images were true positives, recall can be interpreted as the number of relevant items that were actually selected. Since the Fscore takes into account precision as well as recall, it is the preferred confusion matrix analysis metric to gauge the ability of a classifier to predict a class or taxon.

2.3.5 *Plankton concentration estimation and data post processing*

All vignettes collected on the NH-ISIIS transect were classified using the sCNN automated pipeline and the filtering thresholds were applied to remove vignettes with a low confidence classification. Identifications were then merged with the environmental data collected by ISIIS and binned into 1-m vertical bins along the sampling path through the water. The resulting data were used to estimate concentrations of plankton (ind. m^{-3}) and particles based on the volume of water imaged, calculated average tow speed, and time spent by ISIIS in each 1-m vertical stratum.

Finally, because the concentration estimates are based on the total counts from the classifier, which still contain false positive (FP) and false negative (FN) observations, those values need to be adjusted by applying a correction factor (CF_{taxon}). Applying a CF_{taxon} prevents overestimation of concentrations, especially in cases where the FP rates are larger than the FN ones. Since we know these metrics from the Confusion Matrix (CM) analysis, it is possible to calculate a correction factor (*sensu* Hu & Davis, 2006) for each taxon (group) using:

$CF_{taxon} = P_{taxon} / R_{taxon}$ Eq. (4)

Where P_{taxon} and R_{taxon} are estimated for each group using equations 1 and 2, respectively.

ISIIS environmental data were kriged (Matlab package m_krig) onto a grid spanning the length of each transect, at 1-m vertical and 500-m horizontal resolution. ISIIS-derived organismal data were linearly interpolated at a 5-m vertical and 300-m horizontal resolution and used for all biological plots and statistical analyses.

The interpolated biological distribution data of each taxon were used for the hierarchical clustering of their distribution patterns based on longitude, depth, and concentration. To achieve this, all interpolation grid cells were treated as sampling units along the transect. The plankton concentrations found in each of the cells were grouped by taxa and rescaled between zero and one, and then used to build a dissimilarity matrix based on the Sørensen method (*vegdist* function of the "vegan" R-package). To examine similarity among the taxon distributions, we used this dissimilarity matrix to hierarchically cluster the data based on Ward's clustering criterion, using the *hclust* function of the "stats" R-package.

3. Results

3.1 *Environmental setting*

Environmental data revealed a stratified water column across the entire transect (**Fig. 3**), with thermo- and haloclines shoaling toward the shelf. Temperatures ranged between 7.3 ^{o}C at the bottom to 15.6 ^{o}C at the surface (**Fig. 3A**). Surface temperatures were warmer offshore within a feature that extended from the offshore end of the transect to mid-shelf and ~16 m deep. While surface temperatures slowly decreased toward the shelf, values never dropped below 13^{o} C. Salinity followed temperature trends, with values ranging between 30.89 and 33.91 (**Fig. 3B**). A fresher pocket of water, ~0.9 units fresher than the surrounding water in the top 20m (offshore) and in the top 15m (on the shelf) of the water column, was evident in the mid-section of the transect. In waters deeper than ~20 m, the isotherms and isohalines tilted upward towards the coast.

Dissolved oxygen closely followed both thermo- and haloclines, with concentrations ranging from 2.52 to 10.74 mg O_2 L^{-1} (or 1.76-7.52 mL O_2 L^{-1}). A near-hypoxic (*sensu* Peterson et al. 2013) feature was constrained to a single large area at the bottom of the shelf, on the west flank of Stonewall Bank (**Fig. 3C**). A well-defined ~10 m thick and 23.6 km long phytoplankton layer (**Fig. 3D**; as indicated by fluorescence intensity) extended over the shelf to near the shelf break, between ~15 m and ~20 m deep. This chlorophyll-a feature coincided with the depth of the thermocline throughout its length, tilting upward toward the shelf.

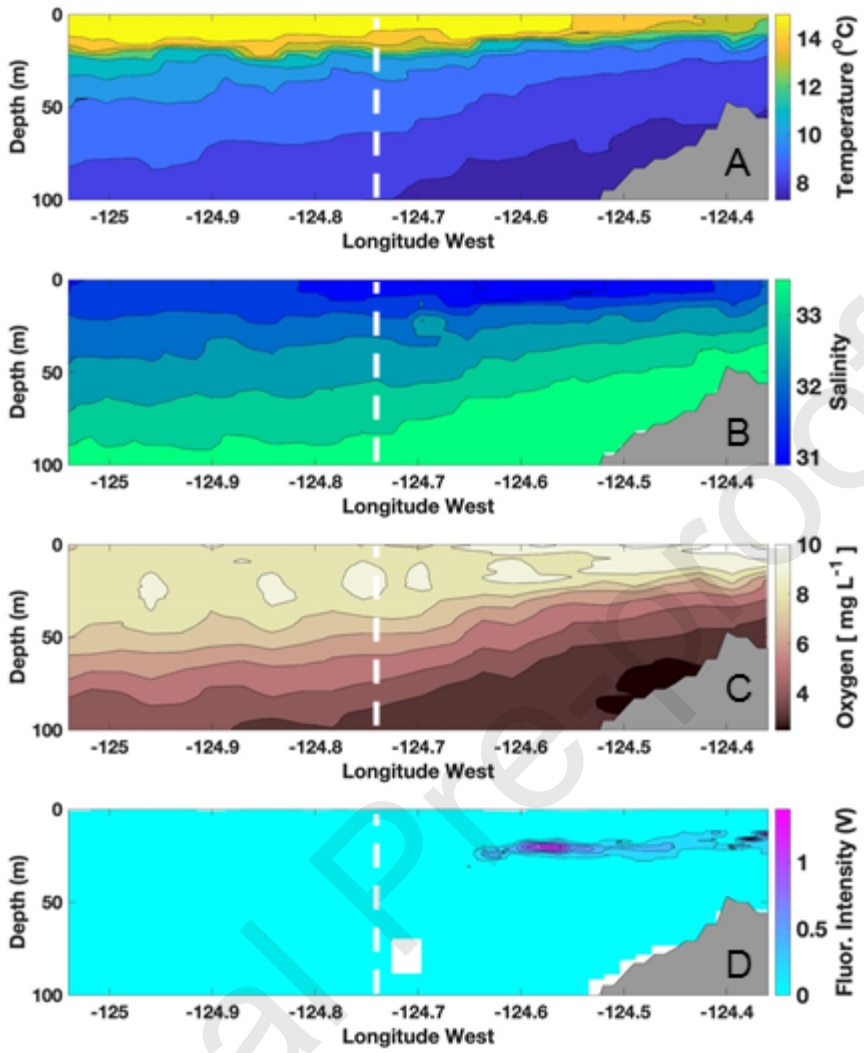

Figure 3. Environmental data sections along the NH-ISIIS line transect. Interpolated data for **A.** Temperature; **B.** Salinity; **C.** Dissolved oxygen (mg O_2 L^{-1}), & **D.** Fluorescence Intensity (V); white box indicates missing data. Gray area represents bathymetry (Stonewall Bank). The dotted white line indicates the shelf break at the 200 m isobath.

3.2 *Sparse convolutional neural network (sCNN)*

After applying filtering thresholds to the 52.4 M vignettes extracted from the NH-ISIIS transect and mapping the 161 original sCNN classes (from the learning library) into 72 broader groups for further ecological analyses, the weighted means of the model precision and recall rates were 83% and 56%, respectively. Notice that these estimates include all groups. Weighted means are reported because the number of images per taxon were not equal in the CM analysis (as should be expected from *in situ* data, which mirrors the system's assemblage relative abundances –for example, there are more images of detritus particles than copepods, but more copepods than teleosts, etc.). The weighted mean F-score (also known as F1-score) of the confusion matrix was 59%. The individual group precision (P_{taxon}), recall (R_{taxon}), and $Fscore_{taxon}$ values are reported in **Supplementary Table 2**).

3.3. *Average plankton and particle concentrations*

The mean concentrations of specific taxa ranged over four orders of magnitude. After phytoplankton (chains 1410.5 ± 33 ind. m^{-3}, mats 187.2 ± 6.5 ind. m^{-3}), several gelatinous taxa were among the taxa with the highest average concentrations along the transect. Appendicularians (66.4 ± 1 ind. m^{-3}), tunicate doliolids (47.6 ± 2 ind. m^{-3}) and budding tunicate doliolids (11.7 ± 1 ind. m^{-3}) were the most abundant. "Copepod other", copepods which were not further identified, were the most abundant crustacean zooplankton with a concentration of 9.9 ± 0.1 ind. m^{-3}, followed by Paracalanidae (8.4 ± 0.1 ind. m^{-3}), "protists other" (7.6 ± 0.1 ind. m^{-3}), and euphausiids (7.1 ± 0.2 ind. m^{-3}). The next most abundant taxa were hydromedusae *Clytia* spp. (6.7 ± 0.5 ind. m^{-3}) and chaetognaths (4.9 ± 0.1 ind. m^{-3}). The small and ubiquitous copepod, *Oithona* spp., had a concentration of 4.6 ± 0.1 ind. m^{-3}, while the most abundant larval fish were myctophids with a concentration of 0.8 ± 0.03 ind. m^{-3} (see **Supplementary Table 3** for other taxa).

3.4. *Fine-scale vertical and horizontal distribution of key taxa along the NH-ISIIS*

3.4.1. *Distribution patterns at high-level taxonomic pooling*

To examine broad taxonomic distributions, data for each group were aggregated to the highest taxonomic level possible (*i.e.*, all fish groups were pooled into "fish larvae", all copepod groups into "copepods", etc.) (**Fig. 4**). While there was some among-group overlap in distributions at this high-level taxonomic "pooling", few taxa groupings exhibited identical distribution patterns.

As an overall group, fish larvae were found mainly offshore with their peak distribution located between 20 and 40 m depth (**Fig. 4A**). This “hotspot” extended from the westernmost end of the transect to the shelf break. A secondary feature, but smaller and with a lower concentration was observed near the bottom and over the shelf on the west flank of Stonewall Bank. Copepods were found throughout the entire transect (**Fig. 4B**). However, their distributions deepened toward the shelf, where they were mostly absent in the top 20 m of the water column. Euphausiids were located mainly in one single large feature between the shelf break and the west flank of Stonewall Bank, with peak concentrations occurring between 60 and 80 m depth (**Fig. 4C**). The concentration hotspot for group “Other crustaceans” overlapped with that of euphausiids; however, the former had a wider cross-shelf distribution, extending over the shelf with a secondary hotspot in the upper water column in offshore waters (**Fig. 4D**).

When pooled at high taxonomic levels, the concentration of gelatinous organisms revealed varying degrees of overlapping distribution patterns. In order of higher to lower concentrations, doliolids (**Fig. 4E**; composed of three different life stages), appendicularians (**Fig. 4F**), and hydromedusae (**Fig. 4G**; encompassing 11 lower taxonomic groups) exhibited the highest concentrations of all gelatinous taxa (hotspots of up to 1000, 400, and 100 individuals m^{-3}, respectively). Their concentrations tended to peak at different locations along the transect: doliolids peaked offshore, appendicularians at the shelf break, and hydromedusae on the shelf, over Stonewall Bank. Chaetognaths (**Fig. 4H**), ctenophores (**Fig. 4I**), and siphonophores (**Fig. 4J**) occurred in lower concentrations (up to 30, 11, and 8 individuals m^{-3}, respectively). Of these, the concentration of chaetognaths and ctenophores peaked over the shelf and on the west flank of Stonewall Bank, with lower concentrations offshore. Siphonophores were present throughout the transect from offshore to the shelf, with peak concentrations in surface waters over the shelf break.

Rhizarians (**Fig. 4K**), a group composed of Foraminifera, acanthereans and radiolarians, were ubiquitous across the transect, with two hotspots (~20 individuals m^{-3}): one offshore, in waters deeper than 40 m, and one over the shelf, in waters shallower than 40 m.

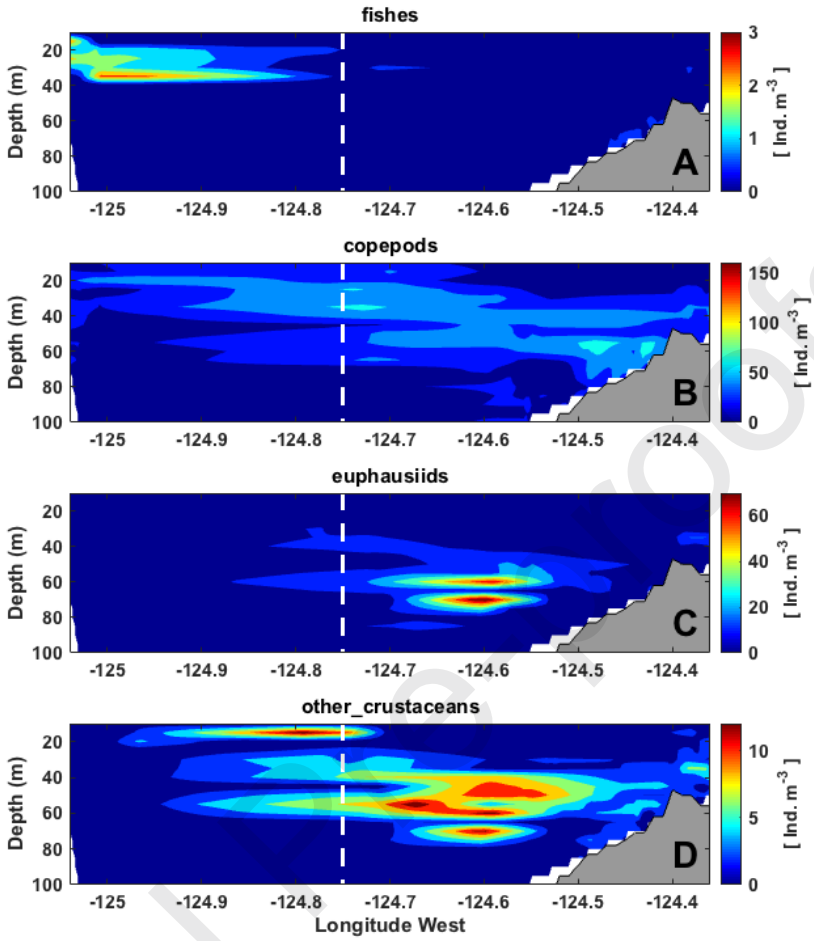

Fig. 4. Aggregated concentration (individuals m^{-3}) distribution for major teleost and crustacean groups: **A.** Fish larvae; **B.** Copepods; **C.** Euphausiids; & **D.** Non-copepod or euphausiid crustaceans (Other crustaceans). The dotted line indicates the shelf break at the 200m isobath.

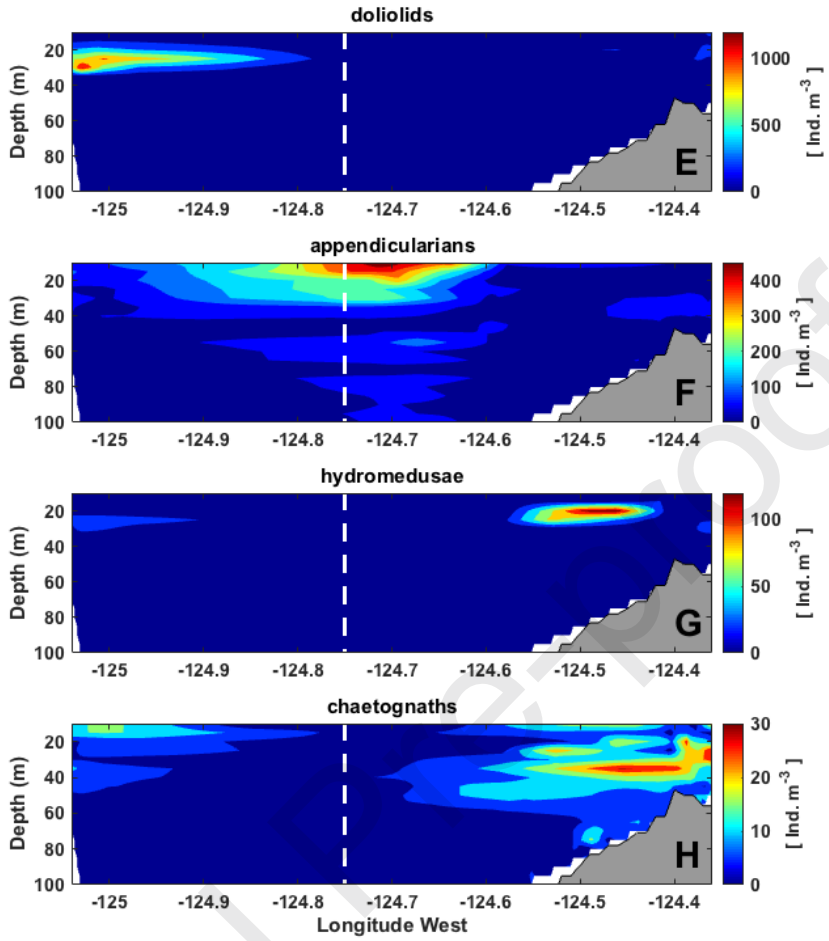

Fig. 4. Aggregated concentration (individuals m^{-3}) distribution for major taxonomic groups: **E.** Doliolids; **F.** Appendicularians; **G.** Hydromedusae; & **H.** Chaetognaths. The dotted line indicates the shelf break at the 200m isobath.

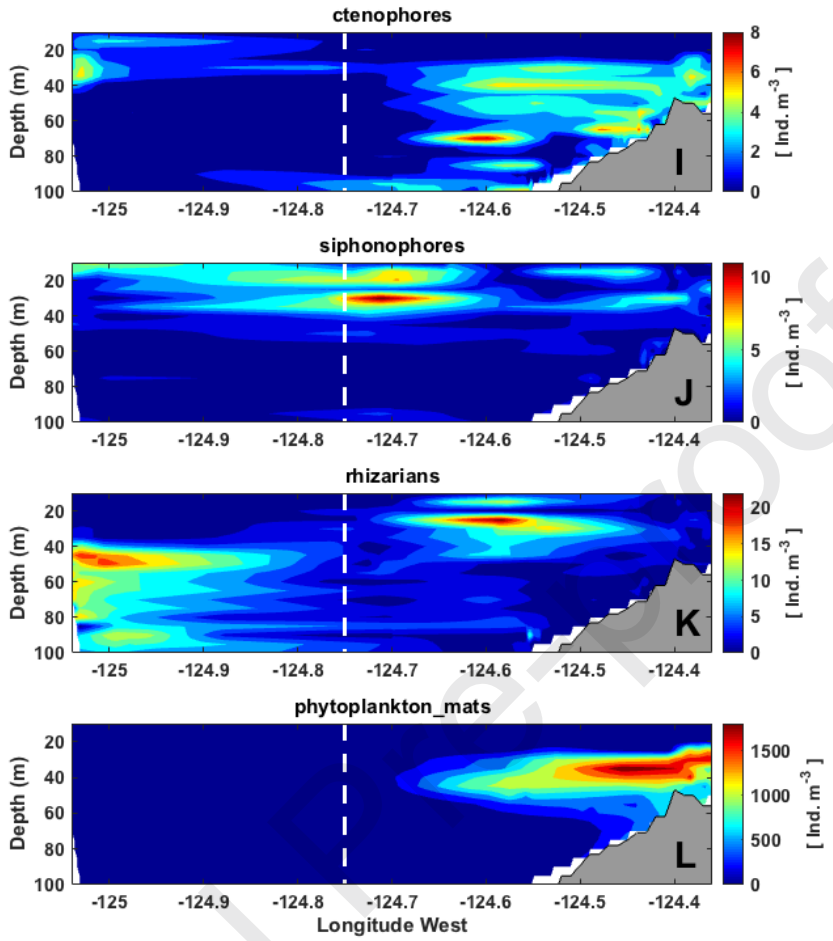

Fig. 4. Aggregated concentration (individuals m^{-3}) distribution for major taxonomic groups: **I.** Ctenophores; **J.** Siphonophores; **K.** Rhizarians (Foraminifera, Acantharia, Radiolaria); & **L.** Phytoplankton mats. The dotted line indicates the shelf break at the 200m isobath.

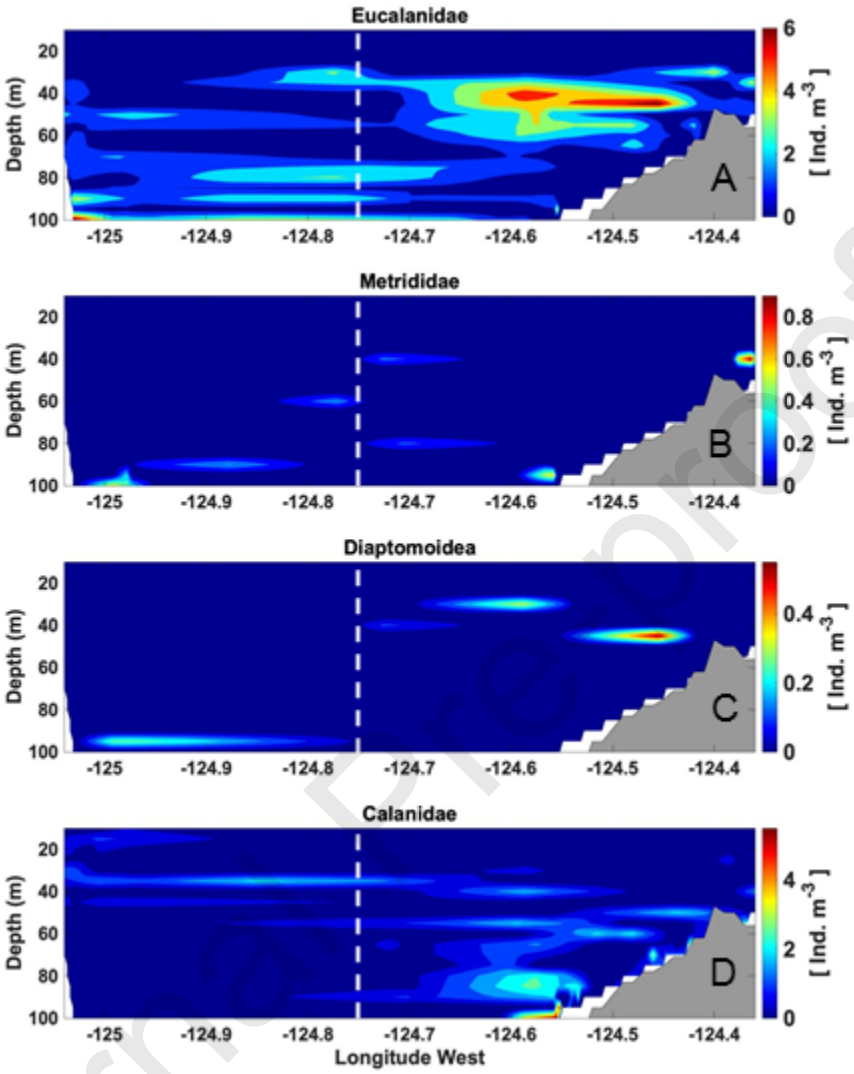

Fig. 5. Main copepod taxa distributions along the NH-ISIIS transect. **A.** Eucalanidae; **B.** Metrididae; **C.** Diaptomoidea; & **D.** Calanidae. The dotted white line indicates the shelf break at the 200 m isobath.

3.4.2. *Distribution patterns at lower-level taxonomic pooling*

We selected copepods (**Fig. 5A-D**) and larval fish (**Fig. 5E-H**) groups to highlight individual group distributions at lower taxonomic levels. Three family (Eucalanidae, Metrididae, and Calanidae) and one super-family (Diaptomoidea) level groups of copepods are shown as

examples. Eucalanidae copepods (**Fig. 5A**) showed a widespread distribution, with their concentrations peaking over the shelf, west of Stonewall Bank, between 60 and 25 m depth. While the concentrations of Calanidae (**Fig. 5D**) peaked at the same longitude as Eucalanidae copepods, the depth of these latter accumulations was 80 m between the shelf break and Stonewall Bank.

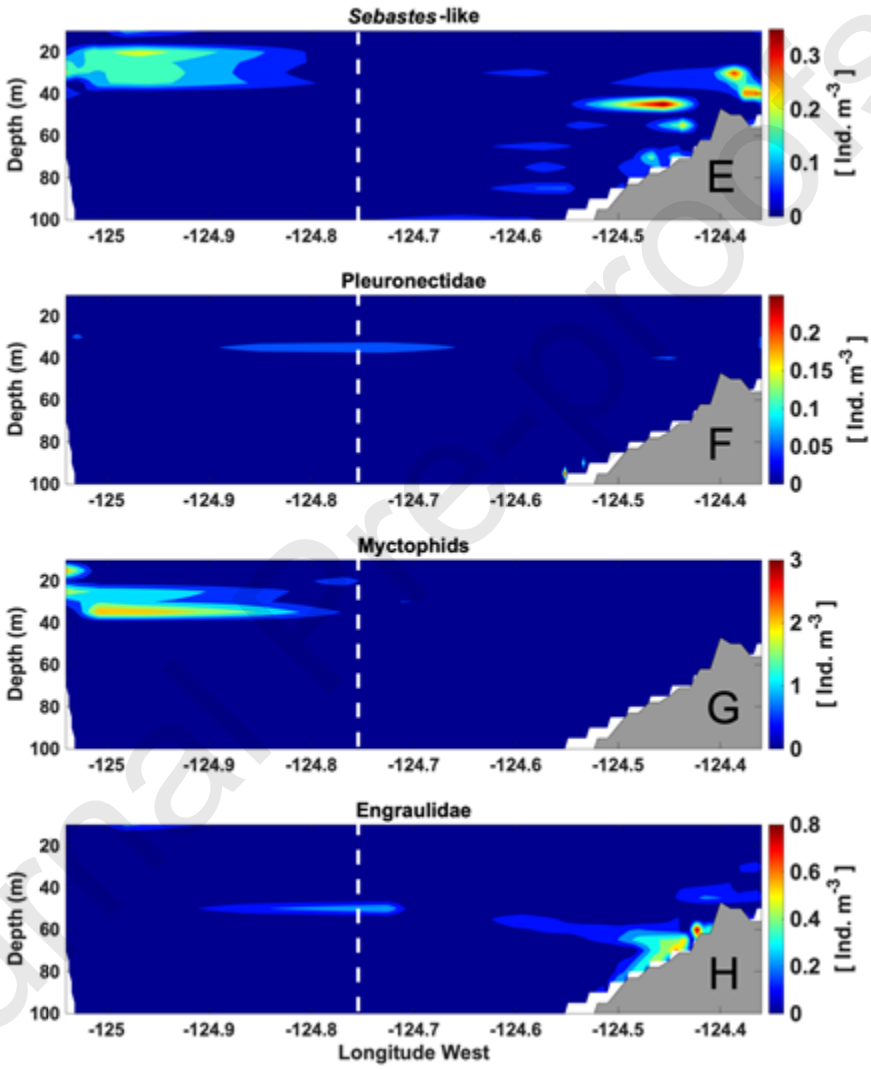

Fig. 5. Example distributions of main fish groups imaged with ISIIS along the NH-ISIIS transect during summer 2016. E. Sebastes-like; F. Pleuronectidae; G. Myctophidae; & H. Engraulidae. The dotted line indicates the shelf break at the 200m isobath.

Four groups of fish larvae (*Sebastes*-like, Pleuronectidae, Myctophidae, and Engraulidae) showed concentration hotspots either offshore, over the shelf break, or on the shelf. *Sebastes*-like larval fishes (**Fig. 5E**) were "patchier" and had higher concentrations over the shelf above Stonewall Bank, in addition to a single larger patch offshore between 20 and 40 m. Pleuronectid fish larvae (**Fig. 5F**), though rare, were found mainly offshore, over the shelf break, almost exclusively at a single depth (~40 m). Myctophids (**Fig. 5G**) were located offshore, where a single large feature with a peak concentration of 3 individuals m^{-3} was located between 20 and 40 m depth. Larval engraulids (**Fig. 5H**) were found offshore at a depth of 50 m, more prominently near the bottom of the western flank of Stonewall Bank.

3.5. *Clustering of taxa based on spatial distribution patterns*

Clustering of the lowest taxonomic level distributions of all taxa along the NH-ISIIS revealed seven distinctly different vertical and horizontal distribution patterns **(Fig. 6**). Cluster 1 included several gelatinous zooplankton, phytoplankton, and protists, among other groups. These taxa were found predominantly in the east, over the shelf, ranging from shallow to mid-depth waters (**Fig. 6, Table 1**). Cluster 2 comprised the most taxa of any cluster, including most copepod taxa as well as euphausiids and appendicularians. The distributions of taxa in this cluster were very broad and complex, with individuals found over most of the water column, and over most of the transect. Cluster 3 included the copepod *Metridia* spp. and copepods of the family Diaptomoidea, both of which were highly patchy, both horizontally and vertically. Cluster 4 included mostly gelatinous plankton as well as crustacean megalopae which were found in low concentrations in shallow waters very close to the transect's easternmost end. Cluster 5 was characterized by taxa with mid-depth distributions as well as distinct, shallow, offshore patches of individuals; included in this cluster were several hydromedusae as well as *Mesocalanus* spp. and some larval fishes. Cluster 6 was characterized by a narrow band of mid-depth distributions. Larval Pleuronectidae (flatfish) and Engraulidae as well as *Pseudocalanus* spp. were members of this cluster. Cluster 7 was characterized by a distinct offshore distribution in shallow (20-40m) waters and comprised larval lanternfish (myctophids) and doliolid tunicates.

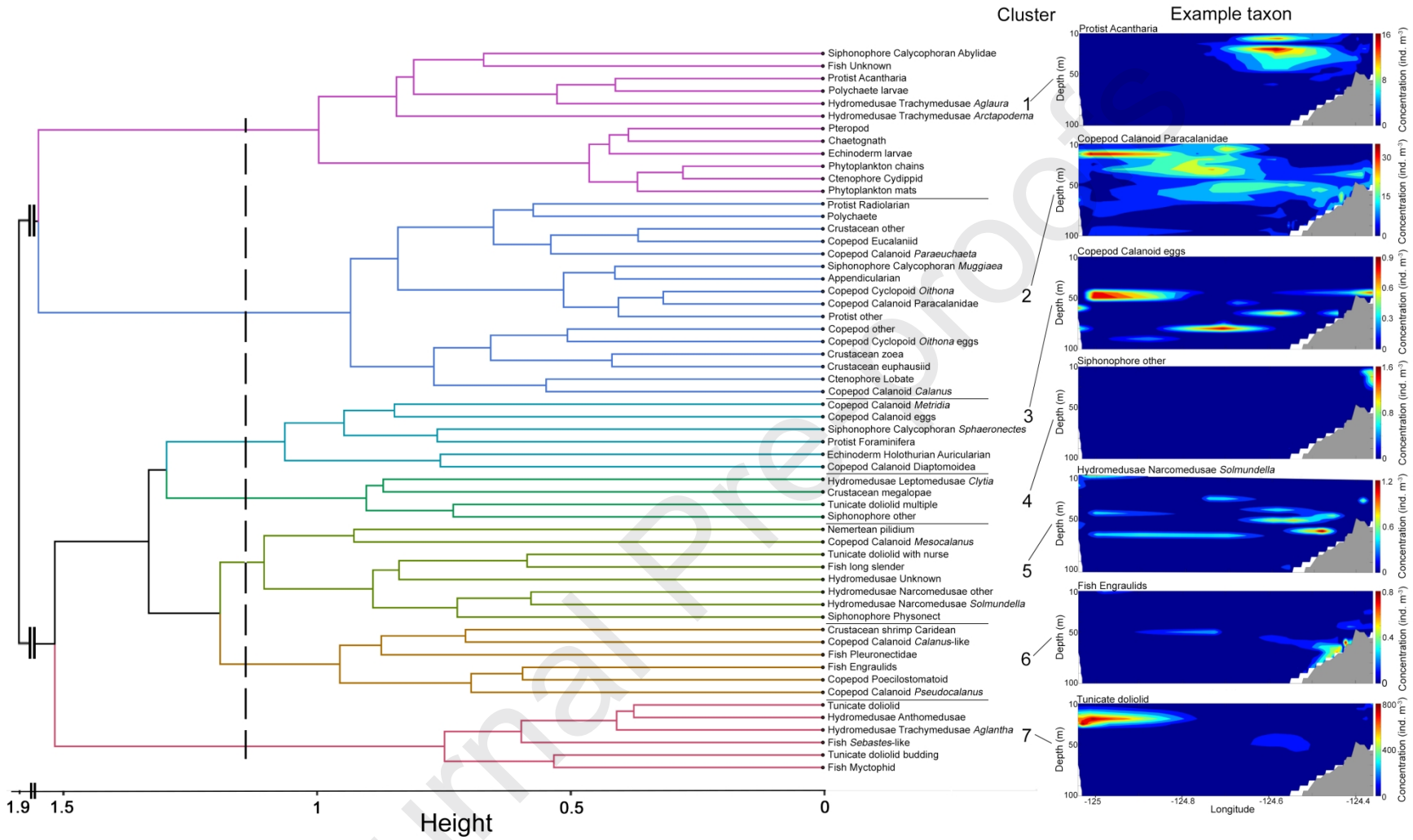

Fig. 6. Dendrogram and clustering for seven groups based on the vertical and cross-shelf distributions of 58 taxa along NH-ISIIS. Example representative distributions for each cluster are shown to the right of the dendrogram.

Table 1. Clusters and their common distribution patterns.

Cluster	Distribution pattern	Taxa in cluster
1	Predominantly eastern, mid-depth to shallow distribution	Siphonophore Calycophoran Abylidae, Fish unknown, Protist Acantharia, Polychaete larvae, Hydromedusae Trachymedusae *Aglaura,* Hydromedusae Trachymedusae *Arctapodema,* Pteropod, Chaetognath, Echinoderm larvae, Phytoplankton chains, Ctenophore Cydippid, Phytoplankton mats
2	Broad and complex horizontal and vertical distributions	Protist Radiolarian, Polychaete, Crustacean adult, Copepod Eucalaniid, Copepod Calanoid *Paraeuchaeta,* Siphonophore Calycophoran *Muggiaea,* Appendicularian, Copepod Cyclopoid *Oithona,* Copepod Calanoid *Paracalanidae,* Protist other, Copepod other, Copepod Cyclopoid *Oithona* eggs, Crustacean zoeae, Crustacean Euphausiid, Ctenophore Lobate, Copepod Calanoid *Calanus*
3	Highly patchy vertically and horizontally	Copepod Calanoid *Metridia,* Copepod Calanoid eggs, Siphonophore Calycophoran *Sphaeronectes,* Protist Foraminifera, Echinoderm Holothurian Auricularian, Copepod Calanoid Diaptomoidea
4	Inshore with individuals near the surface	Hydromedusae Leptomedusae *Clytia,* Crustacean Megalopae, Tunicate doliolid multiple, Siphonophore other
5	Mid-depth, and shallow offshore distribution	Nemertean pilidium, Copepod Calanoid *Mesocalanus,* Tunicate doliolid with nurse, Fish long slender, Hydromedusae unknown, Hydromedusae Narcomedusae other, Hydromedusae Narcomedusae *Solmundella,* Siphonophore Physonect
6	Narrow mid-depth distribution	Crustacean shrimp Caridean, Copepod Calanoid *Calanus*-like, Fish Pleuronectidae, Fish Engraulidae, Copepod Poecilostomatoid, Copepod Calanoid *Pseudocalanus*
7	Offshore and near the surface	Tunicate doliolid, Hydromedusae Anthomedusae, Hydromedusae Trachymedusae *Aglantha,* Fish *Sebastes*-like, Tunicate doliolid budding, Fish Myctophid

4. Discussion

4.1. *Taxonomic & Spatial Resolution*

This was the first deployment of the *In situ* Ichthyoplankton Imaging System (ISIIS) in the northern California Current and the first testing of the image processing and classification pipeline using *in situ* images collected off Oregon. The training library for this region, with its original 161 classes, is to date, the largest and most detailed training library built to classify millions of images in an automated fashion using artificial intelligence methods, such as the sparse Convolutional Neural Network.

The automated classification pipeline allowed us to achieve an unprecedented taxonomic resolution (**Supplementary Table 1**) (see Gorsky et al. 2010; Orenstein et al. 2015 for examples of other imaging studies). In addition, the taxonomic resolution presented here covered a wide range of organisms from protists and different copepods to hydromedusae and siphonophores, with sufficient resolution to compare to previous plankton studies for the region. Moreover, the 161 original classes resulted in 72 groups of differing taxonomic level (phyla, class, family, genera, and in unique cases, to species). Of those, only three were non-biological groups (Artifacts, Detritus & Unknown). In addition, for some groups we were able to resolve different sexes (female copepods carrying eggs such as *Oithona*) or different life stages (e.g., crustacean zoeae, doliolid oozoiods (individuals), phorozoids & nurse stages). These data enabled the mapping of the fine spatial scale distribution of zooplankton (300 m horizontal & 5 m vertical on interpolated data), at different taxonomic or life stage groupings.

4.2. *Physical and environmental properties*

The data for this study were collected in the summer of 2016, the last year of the marine heatwave (“the Blob”), which brought warmer than usual SST temperatures and generally low productivity offshore waters to the continental shelf off central Oregon (Peterson et al. 2017, Brodeur et al. 2019). While at the peak of the phenomenon in 2015 the temperature anomaly was as high as 4.5 ^{o}C (for an observed 19.4 ^{o}C SST), the highest temperature observed in this 2016 study was 15.6 ^{o}C and this was mostly constrained to offshore waters, west of the shelf break. These measurements may indicate that while the system was cooling down, warmer than average surface water temperatures were still present off Newport, OR in June 2016. In addition, isotherm and isohaline lines displayed an upward tilting toward the shelf (deeper

offshore, shallower inshore) while the upper water column was strongly stratified. These conditions are consistent with weak upwelling as reported by Brodeur et al. (2019) for a location 1.5 degrees of latitude south of our sampling location during the same cruise.

Hypoxia off the Oregon coast is a recurring phenomenon (Chan et al. 2008, Peterson et al. 2013, Adams et al. 2016). In addition to the deoxygenated water advected over the shelf during upwelling events (Grantham et al. 2004), new bottom hypoxia pockets associated with biological activity are features now occurring on a seasonal basis on the Oregon coast off Newport (Adams et al. 2013). Understanding how organisms respond to this phenomenon cannot be fully captured with water-column integrating samplers. Along the NH-Line, hypoxia over the shelf develops seasonally, during upwelling conditions, with minimum values (as low as 1.4 ml L^{-1}) recurring between May to late October (Peterson et al. 2013). Our results for the NH-ISIIS are consistent with the latter observations and those of Adams et al. (2016), as indicated by the near-hypoxic (2.52 mg O_2 L^{-1} or 1.76 ml O_2 L^{-1}) pocket sitting over the shelf on the west flank of Stonewall Bank between 60-80 m deep (**Fig. 3**).

4.3. *Physical-Biological Interactions*

The fine vertical resolution of our sampling revealed both biophysical and biological-biological interactions. For example, the near-hypoxic feature on the shelf was located below the highest fluorescence intensity values, which were centered on the pycnocline. In addition, the highest concentrations of phytoplankton mats (**Fig. 4L)** and phytoplankton chains (**Supplementary Fig. 34**) were located 10-30 m below the high fluorescence layer (**Fig. 3D**). These findings indicate that at least some phytoplankton were experiencing flocculation and sinking out of the actively growing phytoplankton layer, and potentially accumulating on the seafloor where their decomposition may have contributed to the low oxygen conditions. Furthermore, while we did not collect water samples to determine the species of diatom forming chains and mats captured in the *in-situ* images, Peterson et al. (2017) reported high abundances of *Pseudo-nitzschia* on the NH-Line in 2016, leading to a toxic bloom. Similar observations of *Pseudo-nitzschia* blooms were made on the NH-Line in the summer of 2015 (Du et al. 2016, Peterson et al. 2017), and as reported for other highly stratified coastal environments (Timmerman et al. 2014, Bowers et al. 2018). Thus, the layer and mats we observed were potentially related to toxin-producing algae such as *Pseudo-nitzschia*.

Organisms have different degrees of tolerance to hypoxic conditions (Vaquer-Sunyer & Duarte, 2008). While most taxa in our study were found in normoxic waters, some groups, including certain copepods (Fig. 4B), ctenophores (Fig. 4I) and fish larvae (Fig. 4A), were found within an hypoxic layer of near-bottom water in the westward flank on Stonewall Bank (Fig. 3C). The copepods found within this hypoxic layer included Paracalanidae (Fig. 6, example taxon for Cluster 2), *Pseudocalanus*, *Oithona* (including egg-carrying females) and Poecilostomatoid copepods (Supplementary Figs. 6, 7, 8, & 10). Although not their optimal, copepods have been found to tolerate (and not avoid) dissolved oxygen concentrations as low as 1 ml L^{-1} (Stalder and Marcus, 1997). The lower oxygen concentration in the near-hypoxic feature observed here was 1.76 mL O_2 L^{-1}, indicating that copepods found within this feature might be able tolerate them. The presence of the ctenophores in the hypoxic conditions is less unusual as many gelatinous organisms including ctenophores are known to be much less affected by low oxygen concentrations (e.g., Breitburg et al. 2003, Kolesar et al. 2010). The near hypoxic conditions found here are considerably lower (<3 mL O_2 L^{-1}) than most teleosts can survive when exposed to low oxygen concentrations over extended periods of time (Ekau et al. 2010). However, two teleost groups (*Sebastes*-like and Engraulidae) were found within this near hypoxic region on the shelf, with the latter occurring in relatively high concentrations directly in the lowest oxygen conditions observed here.

There are two possibilities for these patterns: a) fish larvae could be feeding on copepods or phytoplankton mats. For example, rockfish (*Sebastes*) larvae are known to feed on calanoid and cyclopoid copepods depending on availability (Anderson, 1994). In addition, using isotopic analyses, Bosley et al. (2014) concluded that juvenile coastal rockfish larvae off Oregon had been feeding on primary producers offshore given their depleted ^{13}C signature; this could be another possibility given the overlap of phytoplankton mats (Fig. 4L) in the upper boundary of the near-hypoxic feature. Engraulidae fish larvae can feed on dinoflagellates in laboratory experiments (Lasker et al. 1970), however, stomach contents of fish larvae of some species in the same family have included copepods as the main item (Kumar et al., 2015), while lipid analyses have suggested feeding on calanoid copepods (Håkanson, 1989). An alternative hypothesis is b) that this near-hypoxic layer could be a refuge from predation: a study by Johnson-Colegrove et al. (2015) found that hypoxic conditions only moderately affected fish larvae distributions off Oregon. The alternative explanation of this hypoxic feature being temporary refuge from predation, however, is less clear as some ctenophores could potentially prey on fish larvae. However, it has been reported that interactions between ctenophores, copepods and fish larvae in hypoxic waters are altered, by modifying their behavior and

encounter rates, which affect predation (Kolesar et al. 2010). While our data cannot resolve the underlying dynamics leading to the co-location of these groups, nor the actual interactions given the temporal limitation of our data, it was a very striking observation given the apparent availability of more favorable habitat up in the water column above this near-hypoxic feature or in other areas up- and downslope of Stonewall Bank.

Copepods, as a whole, however, were more typically found in the upper water column west of the shelf break, as well as deeper and below the Chl-*a* layer and phytoplankton mats, farther inshore. The fact that fish larvae, ctenophores, and copepods on the shelf were located below the Chl-*a* layer as well as below the phytoplankton mats and chains, may indicate that these groups were avoiding the layer, possibly due to the abundance of *Pseudo-nitzschia* within the phytoplankton layer (*sensu* Greer et al. 2013). This potential avoidance of surface layers may have pushed taxa distributions to well within the near-hypoxic layer, a phenomenon referred to as hypoxia-based habitat compression (Prince et al. 2010). Previous work using depth-discrete plankton sampling showed that ichthyoplankton off Oregon can have compressed vertical distributions at locations where hypoxic conditions occur (Johnson-Colegrove et al. 2015).

4.4. *Cross-shelf Distribution Patterns & "the Blob"*

There is a paucity of previous taxon-specific three-dimensional distributional data for the region, and one of the goals of this project was to demonstrate that underwater imaging can fill in these gaps. At the same time, it is challenging to compare our highly resolved vertical and horizontal data with depth-integrated net data collected along the stations of the NH-Line. Nonetheless, the cluster analysis carried out here revealed several spatial patterns that correspond with previously reported data in terms of cross-shelf distributions along the NH-Line (Keister & Peterson, 2003), or the presence of key copepod taxa in time series analyses, such as the interannual variability of copepods at NH-Line station number 05 or NH05 (Peterson & Keister, 2003; see also Fig. 1A for the station location along the line).

To detect patterns in the cross-shelf distributions of different taxa, the cluster analysis was based on spatially-explicit parameters of longitude and depth. Cluster 1 represented taxa that were found between the shelf break and the western flank of Stonewall Bank in waters that were also occupied by phytoplankton mats. These mats, as discussed earlier, are likely composed of *Pseudo-nitzschia* (a domoic acid-producing diatom), which could induce an

avoidance behavior in copepods (Greer et al. 2013), and may explain why no copepods were found in Cluster 1. However, gelatinous groups known to prey on copepods were also found in this cluster, confounding the domoic acid-avoidance hypothesis as it is also possible that copepods could be avoiding their gelatinous predators (Greer et al. 2013). Further, our sampling occurred only during daylight hours, thus it is not possible to speculate on whether copepods were avoiding these shallower depths simply due to diel vertical migration behavior (Cohen and Forward, 2009). However, copepods were found at similar depths offshore, where phytoplankton mats and possibly *Pseudo-nitzschia* were absent, indicating that avoidance of these phytoplankton features is likely.

Several abundant copepod taxa (e.g., *Calanus* and *Oithona*) were found in Cluster 2, which was characterized by broad horizontal and vertical distributions. While we cannot distinguish which *Calanus* species were present (i.e. whether they were cold neritic species or warm oceanic species), *Oithona* is a ubiquitous representative and can be found in both summer and winter communities (Peterson & Miller, 1977). *Metridia* sp. on the other hand has been classified as a “Transitional Group” (Keister & Peterson, 2003) and as typically occurring in “Cold-water, offshore” (Peterson & Keister, 2003). In our cluster analysis, *Metridia* (a group with a high F-score of 0.99; **Supplementary table 2**) was part of Cluster 3, a group with scattered patches mainly in deep, cold waters, but was also present over the shelf in mid-depth (and not in the warmer surface waters (**Fig. 5B**). The juxtaposition of these two clusters reflects a scenario that would be expected during the transition from warm water temperatures to typical colder conditions.

Cluster 4 contained taxa that were very rare and were only found in the easternmost parts of the transect. This cluster included crustacean megalopae. Although we cannot definitively identify the species, given the timing of sampling (late June), it is possible that the economically important Dungeness crab (*Cancer magister*) were a major constituent of this group. Dungeness crab are an important fishery off the OR coast, and megalopae recruitment strength has been shown to be a good indicator of subsequent fishery catch (Shanks et al. 2010). While the largest Dungeness crab recruitment events typically occur April-May in Oregon, the recruitment season often extends through August in lower abundances (Rasmuson, 2013).

Taxa with narrow bands of mid-depth distributions were found in Cluster 6, and one of the taxa in this group was the copepod *Mesocalanus* sp. Although identification to species level was not possible, the only abundant *Mesocalanus* reported for this region is *Mesocalanus*

tenuicornis (e.g., Fisher et al. 2015). While typically a species found in the waters off central and southern California (Mackas et al. 2001, Hooff & Peterson, 2006), the copepod has been found off the central Oregon coast when warm subtropical water infiltrates the usually colder coastal waters (Fisher et al. 2015). Thus, the observation of *Mesocalanus* is consistent with the persistence of the warm water anomaly recorded off the Oregon coast (Peterson et al. 2017), which was winding down, but was still detectable in 2016 (Brodeur et al. 2019).

Another copepod group in our dataset, *Pseudocalanus* (0.99 F-score), was also grouped in Cluster 6 (Narrow, mid-depth distribution, Table 1). Although previously classified as "Offshore summer/everywhere winter" (Keister & Peterson, 2003), in the present study, *Pseudocalanus* copepods were found in highest concentrations on the west flank of Stonewall Bank, with lower concentrations offshore, in deep waters west of the shelf break (Supplementary Fig. 6).

Consistent with earlier studies (e.g., Auth and Brodeur, 2006), larval myctophids were found exclusively west of the shelf break (Cluster 7; **Fig. 6; Table 1**), which is likely linked to the habitat of adult populations and thus spawning locations. *Sebastes*-like larvae were found both offshore and close to shore which is consistent with the broad cross-shelf distributions of various rockfish species. Engraulids (most likely northern anchovy *Engraulis mordax*) were found close to shore which is generally not the normal distribution of this group, but during these anomalous ocean conditions, their distribution patterns appeared to be skewed much closer to shore (Auth et al. 2018).

The unusually warm water temperatures associated with the presence of the "Blob" off the Oregon coast were accompanied by a positive biomass anomaly of "southern" species (Peterson et al. 2015b). Our 2016 cruise also followed an El Niño and a strong, warm PDO (Peterson et al. 2015a, b), and not surprisingly, ISIIS environmental sensors recorded warmer than usual temperatures. Most of the taxa clustered in the "El Niño" group of Keister & Peterson (2003) were also found in our imagery data: for example, Eucalanoidea, Diaptomoidea and Calanidae copepods, physonect & calycophoran siphonophores, ctenophores, and appendicularians (**Fig. 4**; see other groups in supplementary materials). These data reinforce the persistent occurrence in 2016 of warm water species along the NH-ISIIS transect. In a concurrent study, Brodeur et al. (2019) also reported a significant increase in gelatinous macrozooplankton. While ISIIS cannot image taxa as large as those sampled by Brodeur et al. (2019), *in-situ* imaging is very well suited for smaller gelatinous zooplankton, especially mesozooplankton-sized ones, as the plankton is not disturbed during imaging. Net sampling on

the other hand often damages or destroys gelatinous individuals and can lead to undersampling (Remsen et al. 2004, Hosia et al. 2017). The high concentrations of smaller gelatinous organisms (several hydromedusae, doliolids, and appendicularians) found in our images, especially offshore, may indicate that a similar increase in the abundance of these taxa likely occurred. As such distribution and abundance data for this region are novel, a similar high-resolution comparison to “normal” years is necessary to establish whether or not our observed concentrations for gelatinous groups were anomalously high.

4.5 *Concluding Remarks*

In this study, we were able to describe the fine-scale vertical and horizontal distributions of key plankton taxa along the NH-ISIIS, just south of the NH-Line. The NH-Line time series has produced and will continue to produce ecologically valuable information as stations are regularly sampled from near the seafloor (or from 100 m in deeper water) to the surface, using oblique ring net tows. The addition of sampling with a high-resolution imaging system, such as used in this study, offers the combined benefit of a wide taxonomic range and fine-scale spatial resolution needed to better understand the physical-biological interactions shaping planktonic distributions. When applied to a broader spatial context, we envision not only complimenting the time series conducted on the NH-Line, but also resolving processes driving plankton seascapes within the Northern California Current (*sensu* Kavanaugh et al. 2016).

Acknowledgements

This study was made possible by the opportunity to join the NOAA-funded Pre-Recruit Survey cruise. During the preparation of this manuscript, C.B., M.S, S.S. and R.K.C. were supported by NSF OCE 1737399 to R.K. Cowen and S. Sponaugle. We thank Kelly Robinson, University of Louisiana Lafayette, for her help with the field work. Christopher Sullivan and Michaela Buchanan from Oregon State University’s Center for Genomic Research and Biocomputing assisted with image processing and pipeline implementation on their GPU infrastructure. We thank the officers and crew of the NOAA ship *Bell M. Shimada* for their professionalism at sea and their help with deployments.

References

Adams, K.A., Barth, J.A., Chan, F., 2013. Temporal variability of near-bottom dissolved oxygen during upwelling off central Oregon. J. Geophys. Res. Ocean. 118, 4839–4854. https://doi.org/10.1002/jgrc.20361

Adams, K.A., Barth, J.A., Shearman, R.K., 2016. Intraseasonal cross-shelf variability of hypoxia along the Newport, Oregon, Hydrographic Line. J. Phys. Oceanogr. 46, 2219–2238. https://doi.org/10.1175/JPO-D-15-0119.1

Anderson, J.T. 1994. Feeding ecology and condition of larval and pelagic juvenile redfish *Sebastes* spp. Mar. Ecol. Progr. Ser. 104: 211-226. https://doi.org/10.3354/meps104211

Auth, T.D., Brodeur, R.D., 2006. Distribution and community structure of ichthyoplankton off the coast of Oregon, USA, in 2000 and 2002. Mar. Ecol. Prog. Ser. 319, 199–213. https://doi.org/10.3354/meps319199

Auth, T.D., Brodeur, R.D., Soulen, H.L., Ciannelli, L., Peterson, W.T., 2011. The response of fish larvae to decadal changes in environmental forcing factors off the Oregon coast. Fish. Oceanogr. 20(4), 314-328.

Auth, T.D., Daly, E.A., Brodeur, R.D., Fisher, J.L., 2018. Phenological and distributional shifts in ichthyoplankton associated with recent warming in the northeast Pacific Ocean. Glob. Chang. Biol. 24, 259–272. https://doi.org/10.1111/gcb.13872

Bond, N.A., Cronin, M.F., Freeland, H., Mantua, N. (2015) Causes and impacts of the 2014 warm anomaly in the NE Pacific. Geophys. Res. Lett. 42, 3414–3420, doi:10.1002/2015GL063306.

Bosley, K.L., Miller, T.W., Brodeur, R.D., Bosely, K.M., Gaest, A.V., Elz, A. 2014. Feeding ecology of juvenile rockfishes off Oregon and Washington based on stomach content and stable isotope analyses. Mar. Biol. 161: 2381-2393. https://doi.org/10.1007/s00227-014-2513-8

Bowers, H.A., Ryan, J.P., Hayashi, K., Woods, A.L., Marin, R III, Smith, G.J., Hubbard, K.A., Doucette, G.J., Mikulski, C.M., Gellene, A.G., Zhang, Y., Kudela, R.M., Caron, D.A., Birch, J.M., Scholin, C.A., 2018. Diversity and toxicity of *Pseudo-nitzschia* species in Monterey Bay: Perspectives from targeted and adaptive sampling. Harmful Alagae, 78, 129-141. https://doi.org/10.1016/j.hal.2018.08.006.

Breitburg, D.L., Adamack, A., Kolesar, S.E., Decker, M.B., Rose, K.A.,Purcell, J.E., Keister, J.E., Cowan, J.H. 2003 The pattern and influence of low dissolved oxygen in the Patuxent River, a seasonally hypoxic estuary. Estuaries 26, 280–297.

Brodeur, R.D., Peterson, W.T., Auth, T.D., Soulen, H.L., Parnel, M.M., Emerson, A.A., 2008. Abundance and diversity of coastal fish larvae as indicators of recent changes in ocean and climate conditions in the Oregon upwelling zone. Mar. Ecol. Prog. Ser. 366, 187-202.

Brodeur, R.D., Auth, T.D., Phillips, A.J., 2019. Major shifts in pelagic micronekton and macrozooplankton community structure in an upwelling ecosystem related to an unprecedented marine heatwave. Front. Mar. Sci. 6, 212. https://doi.org/10.3389/FMARS.2019.00212

Chan, F., Barth, J.A., Lubchenco, J., Kirincich, A., Weeks, H., Peterson, W.T., Menge, B.A., 2008. Emergence of anoxia in the California current large marine ecosystem. Science 319 (5865), 920. https://doi.org/10.1126/science.1149016

Childers, J., Snyder, S., Kohin, S., 2011. Migration and behavior of juvenile North Pacific albacore (*Thunnus alalunga*). Fish. Oceanogr. 20, 157–173. https://doi.org/10.1111/j.1365-2419.2011.00575.x

Cohen, J.H., Forward, R.B.J., 2009. Zooplankton diel vertical migration — A review of proximate control. Oceanogr. Mar. Biol. Annu. Rev. 47, 77–109.

Cowen, R.K., Greer, A.T., Guigand, C.M., Hare, J.A., Richardson, D.E., Walsh, H.J., 2013. Evaluation of the In Situ Ichthyoplankton Imaging System (ISIIS): Comparison with the traditional (bongo net) sampler. Fish. Bull. 111. https://doi.org/10.7755/FB.111.1.1

Cowen, R.K., Guigand, C.M., 2008. In situ ichthyoplankton imaging system (ISIIS): System design and preliminary results. Limnol. Oceanogr. Methods 6, 126–132. https://doi.org/10.4319/lom.2008.6.126

Davis, C.S., Thwaites, F.T., Gallager, S.M., Hu, Q., 2005. A three-axis fast-tow digital Video Plankton Recorder for rapid surveys of plankton taxa and hydrography. Limnol. Oceanogr. Methods 3, 59–74. https://doi.org/10.4319/lom.2005.3.59

Dieleman, S., De Fauw, J., Kavukcuoglu, K., 2016. Exploiting cyclic symmetry in convolutional neural networks.

Du, X., Peterson, W., Fisher, J., Hunter, M., Peterson, J., 2016. Initiation and development of a toxic and persistent *Pseudo-nitzschia* bloom off the Oregon coast in spring/summer 2015. PLoS One 11, e0163977. https://doi.org/10.1371/journal.pone.0163977

Ekau, W., Auel, H., Pörtner, H.-O., Gilbert, D. Impacts of hypoxia on the structure and processes in pelagic communities (zooplankton, macro-invertebrates and fish). Biogeosci. 7: 1669-1699. https://doi.org/ 10.5194/bg-7-1669-2010

Faillettaz, R., Picheral, M., Luo, J.Y., Guigand, C., Cowen, R.K., Irisson, J-O., 2016. Imperfect automatic image classification successfully describes plankton distribution patterns. Methods Oceanogr. 15–16, 60–77. https://doi.org/10.1016/J.MIO.2016.04.003

Fisher, J.L., Peterson, W.T., Rykaczewski, R.R., 2015. The impact of El Niño events on the pelagic food chain in the northern California Current. Glob. Chang. Biol. 21, 4401–4414. https://doi.org/10.1111/gcb.13054

Francis, T.B., Scheuerell, M.D., Brodeur, R.D., Levin, P.S., Ruzicka, J.J., Tolimieri, N., Peterson, W.T., 2012. Climate shifts the interaction web of a marine plankton community. Glob. Change Biol. 18, 2498-2508.

Gorsky, G., Ohman, M.D., Picheral, M., Gasparini, S., Stemmann, L., Romagnan, J.-B., Cawood, A., Pesant, S., Garcia-Comas, C., Prejger, F., 2010. Digital zooplankton image analysis using the ZooScan integrated system. J. Plankton Res. 32, 285–303. https://doi.org/10.1093/plankt/fbp124

Graham, B., 2015. Fractional max-pooling. arXiv preprint arXiv:1412.6071.

Grantham, B.A., Chan, F., Nielsen, K.J., Fox, D.S., Barth, J.A., Huyer, A., Lubchenco, J., Menge, B.A., 2004. Upwelling-driven nearshore hypoxia signals ecosystem and oceanographic changes in the northeast Pacific. Nature 429, 749–754. https://doi.org/10.1038/nature02605

Greer, A.T., Cowen, R.K., Guigand, C.M., McManus, M.A., Sevadjian, J.C., Timmerman, A.H.V. 2013. Relationships between phytoplankton thin layers and the fine-scale vertical distributions of two trophic levels of zooplankton. J. Plankton Res. 35, 939–956. https://doi.org/10.1093/plankt/fbt056

Håkanson, J.L.1989. Condition of larval anchovy (*Engraulis mordax*) in the Southern California Bight, as measured through lipid analysis. Mar. Biol. 102, 153-159.

Hobday, A.J., Oliver, E.C.J., Sen Gupta, A., Benthuysen, J.A., Burrows, M.T., Donat, M.G., Holbrook, N.J., Moore, P.J., Thomsen, M.S., Wernberg, T., Smale, D.A. 2018. Categorizing and naming marine heatwaves. Oceanography 31, 162-173.

Hooff, R.C., Peterson, W.T., 2006. Copepod biodiversity as an indicator of changes in ocean and climate conditions of the northern California current ecosystem. Limnol. Oceanogr. 51, 2607–2620. https://doi.org/10.4319/lo.2006.51.6.2607

Hosia, A., Falkenhaug, T., Baxter, E.J., Pagès, F., 2017. Abundance, distribution and diversity of gelatinous predators along the northern Mid-Atlantic Ridge: A comparison of different sampling methodologies. PLoS One 12, e0187491. https://doi.org/10.1371/journal.pone.0187491

Hu, Q., Davis, C., 2006. Accurate automatic quantification of taxa-specific plankton abundance using dual classification with correction. Mar. Ecol. Prog. Ser. 306, 51–61. https://doi.org/10.2307/24869900

Johnson-Colegrove, A., Ciannelli, L., Brodeur, R.D., 2015. Ichthyoplankton distribution and abundance in relation to nearshore dissolved oxygen levels and other environmental variables within the Northern California Current System Fish. Oceanogr. 24, 495–507.

Kavanaugh, M.T., Oliver, M.J., Chavez, F.P., Letelier, R.M., Muller-Karger, F.E., Doney, S.C., 2016. Seascapes as a new vernacular for pelagic ocean monitoring, management and conservation. ICES J. Mar. Sci. J. du Cons. 73, 1839–1850. https://doi.org/10.1093/icesjms/fsw086

Keister, J., Di Lorenzo, E., Morgan, C., Combes, V., Peterson, W., 2011. Zooplankton species composition is linked to ocean transport in the northern California Current. Glob. Chang. Biol. 17, 2498–2511. https://doi.org/10.1111/j.1365-2486.2010.02383.x

Keister, J.E., Peterson, W.T., 2003. Zonal and seasonal variations in zooplankton community structure off the central Oregon coast, 1998–2000. Prog. Oceanogr. 57, 341–361. https://doi.org/10.1016/S0079-6611(03)00105-8

Kolesar, S.E., Breitburg, D.L., Purcell, J.E., Decker, M.B. 2010. Effects of hypoxia on Mnemiposis leidyi, ichthyoplankton, and copepods: clearance rates and vertical habitat overlap. Mar. Ecol. Progr. Ser. 411: 173-188. https://doi.org/10.3354/meps08656

Kumar, M.A., Padmavati, G., and Venu, S. 2015. Food and Feeding Dynamics of *Stolephorus commersonnii* (Lacepede, 1803) (Family: Engraulidae) from South

Andaman. J. Mar. Biol., Article ID 870919, 8 pages, https://dx.doi.org/10.1155/2015/870919

Lasker, R., Feder, H.M., Theilacker, G.H., and May, R.C. 1970. Feeding, growth, and survival of *Engraulis mordax* larvae reared in the laboratory. Mar. Biol. 5, 345-353.

LeCun, Y., Bengio, Y., Hinton, G., 2015. Deep learning. Nature 521, 436–444. https://doi.org/10.1038/nature14539

Lombard, F., et al. 2019. Globally consistent quantitative observations of planktonic ecosystems. Front. Mar. Sci. https://doi.org/10.3389/fmars.2019.00196

Luo, J.Y., Grassian, B., Tang, D., Irisson, J-O., Greer, A.T., Guigand, C.M., McClatchie, S., Cowen, R.K., 2014. Environmental drivers of the fine-scale distribution of a gelatinous zooplankton community across a mesoscale front. Mar. Ecol. Prog. Ser. 510, 129–149. https://doi.org/10.3354./mesp10908

Luo, J.Y., Irisson, J-O., Graham, B., Guigand, C., Sarafraz, A., Mader, C., Cowen, R.K., 2018. Automated plankton image analysis using convolutional neural networks. Limnol. Oceanogr. Methods 16, 814–827. https://doi.org/10.1002/lom3.10285

Mackas, D.L., Thomson, R.E., Galbraith, M., 2001. Changes in the zooplankton community of the British Columbia continental margin, 1985-1999, and their covariation with oceanographic conditions. Can. J. Fish. Aquat. Sci. 58, 685–702. https://doi.org/10.1139/f01-009

McClatchie, S., Cowen, R., Nieto, K., Greer, A., Luo, J.Y., Guigand, C., Demer, D., Griffith, D., Rudnick, D., 2012. Resolution of fine biological structure including small narcomedusae across a front in the Southern California Bight. J. Geophys. Res. Ocean. 117, 1–18. https://doi.org/10.1029/2011JC007565

Orenstein, E., Beijbom, O., Peacock, E., Sosik, H. 2015. WHOI-Plankton- A Large Scale Fine Grained Visual Recognition Benchmark Dataset for Plankton Classification. arXiv preprint arXiv:1510.00745

Peterson, J.O., Morgan, C.A., Peterson, W.T., Lorenzo, E. Di, 2013. Seasonal and interannual variation in the extent of hypoxia in the northern California Current from 1998-2012. Limnol. Oceanogr. 56, 2279–2292 https://doi.org/10.4319/lo.2013.58.6.2279

Peterson, W.T., Fisher, J.L., Peterson, J.O., Morgan, C.A., Burke, B.J., Fresh, K.L., 2014. Applied fisheries oceanography: Ecosystem indicators of ocean conditions inform fisheries management in the California Current. Oceanography 27, 80–89.

Peterson, W.T., Keister, J.E., Feinberg, L.R., 2002. The effects of the 1997–99 El Niño/La Niña events on hydrography and zooplankton off the central Oregon coast. Prog. Oceanogr. 54, 381–398. https://doi.org/10.1016/S0079-6611(02)00059-9

Peterson, W.T., Fisher, J.L., Strub, P.T., Du, X., Risien, C., Peterson, J., Shaw, C.T., 2017. The pelagic ecosystem in the Northern California Current off Oregon during the 2014-2016 warm anomalies within the context of the past 20 years. J. Geophys. Res. Ocean. 122, 7267–7290. https://doi.org/10.1002/2017JC012952

Peterson, W.T., Keister, J.E., 2003. Interannual variability in copepod community composition at a coastal station in the northern California Current: A multivariate

approach. Deep Sea Res. 50, 2499–2517. https://doi.org/10.1016/S0967-0645(03)00130-9

Peterson, W.T., Miller, C.B., 1975. Year-to-year variations in the planktology of the Oregon upwelling zone. Fish. Bull. 73, 642–653

Peterson, W.T., Robert, M., Bond, N., 2015a. The warm Blob- Conditions in the northeastern Pacific Ocean. PICES Press 23, 36-38.

Peterson, W.T., Robert, M., Bond, N., 2015b. The warm Blob continues to dominate the ecosystem of the northern California Current. PICES Press 23, 44-46.

Peterson, W.T., Miller, C., 1977. Seasonal cycle of zooplankton abundance and species composition along the central Oregon coast. Fish. Bull. 75, 717–724.

Phillips, A.J., Ciannelli, L., Brodeur, R.D., Pearcy, W.G., Childers, J., 2014. Spatio-temporal associations of albacore CPUEs in the Northeastern Pacific with regional SST and climate environmental variables. ICES J. Mar. Sci. 71, 1717–1727. https://doi.org/10.1093/icesjms/fst238

Picheral, M., Guidi, L., Stemmann, L., Karl, D.M., Iddaoud, G., Gorsky, G., 2010. The Underwater Vision Profiler 5: An advanced instrument for high spatial resolution studies of particle size spectra and zooplankton. Limnol. Oceanogr. Methods 8, 462–473. https://doi.org/10.4319/lom.2010.8.462

Prairie, J.C., Sutherland, K.R., Nicklos, K.J., Kaltenberg, A.M., 2012. Biophysical interactions in the plankton: A cross-scale review. Limnol. Oceanogr. Fluids Environ. 2, 121-145. https://doi.org/10.1215/21573689-1964713

Prince, E., Luo, J., Goodyear, C., Hoolihan, J., Snodgrass, D., Orbesen, E., Serafy, J., Ortiz, M., Schirripa, M., 2010. Ocean scale hypoxia-based habitat compression of Atlantic istiophorid billfishes. Fish. Oceanogr. 19, 448–462. https://doi.org/10.1111/j.1365-2419.2010.00556.x

Remsen, A., Hopkins, T.L., Samson, S., 2004. What you see is not what you catch: A comparison of concurrently collected net, Optical Plankton Counter, and Shadowed Image Particle Profiling Evaluation Recorder data from the northeast Gulf of Mexico. Deep Sea Res. Part I Oceanogr. Res. Pap. 51, 129–151. https://doi.org/10.1016/J.DSR.2003.09.008

Rasmuson, L.K. 2013. The Biology, Ecology and Fishery of the Dungeness crab, *Cancer magister*. Adv. Mar. Biol. 65, 95-148. https://doi.org/10.1016/B978-0-12-410498-3.00003-3

Richardson, D.E., Llopiz, J.K., Leaman, K.D., Vertes, P.S., Muller-Karger, F.E., Cowen, R.K., 2009. Sailfish (*Istiophorus platypterus*) spawning and larval environment in a Florida Current frontal eddy. Prog. Oceanogr. 82, 252–264. https://doi.org/10.1016/j.pocean.2009.07.003

Robinson, K.L., Luo, J.Y., Sponaugle, S., Guigand, C., Cowen, R.K., 2017. A tale of two crowds: Public engagement in plankton classification. Front. Mar. Sci. 4, 82. https://doi.org/10.3389/fmars.2017.00082

Schmid, M.S., Fortier, L., 2019. The intriguing co-distribution of the copepods *Calanus hyperboreus* and *Calanus glacialis* in the subsurface chlorophyll maximum of Arctic seas. Elem. Sci. Anthr. (in review).

Schmid, M.S., Maps, F., Fortier, L., 2018. Lipid load triggers migration to diapause in Arctic Calanus copepods—insights from underwater imaging. J. Plankton Res. 40, 311–325. https://doi.org/10.1093/plankt/fby012

Schmid, M.S., Aubry, C., Grigor, J., Fortier, L., 2016. The LOKI underwater imaging system and an automatic identification model for the detection of zooplankton taxa in the Arctic Ocean. Methods Oceanogr. 15–16, 129–160. https://doi.org/10.1016/J.MIO.2016.03.003

Shanks, A.L., Roegner, G.C., 2007. Recruitment limitation in Dungeness crab populations is driven by variation in atmospheric forcing. Ecology 88, 1726–1737. https://doi.org/10.1890/06-1003.1

Shanks, A., Roegner, G.C., and Miller, J. 2010. Using megalopae to predict future commercial catches of Dungeness crabs (*Cancer magister*) in Oregon. CalCOFI Rep. 51, 106-118.

Tharwat, A., 2018. Classification Assessment Methods. Applied Computing and Informatics. https://doi.org/10.1016/j.aci.2018.08.003

Timmerman, A.H.V., McManus, M.A., Cheriton, O. M. Cowen, R.K., Greer, A.T., Kudela, R.M., Ruttenberg, K., Sevadjian, J., 2014. Hidden thin layers of toxic diatoms in a coastal bay. Deep Sea Res. II: Topical Studies in Oceanogr. 101: 129-140. https://doi.org/10.1016/j.dsr2.2013.05.030

Vaquer-Sunyer, R., Duarte, C.M., 2008. Thresholds of hypoxia for marine biodiversity. Proc. Natl. Acad. Sci. 105, 15452–15457. https://doi.org/10.1073/PNAS.0803833105

Wiebe, P.H., Benfield, M.C., 2003. From the Hensen net toward four-dimensional biological oceanography. Prog. Oceanogr. 56, 7–136. https://doi.org/10.1016/S0079-6611(02)00140-4

Author Contributions

Christian Briseño-Avena & Moritz Schmid led the manuscript. All authors contributed equally to reviewing and editing the manuscript.

Competing interests

The authors declare no competing interests.

Supplementary Information

This manuscript is accompanied by Supplementary Figures 1-49 as well as three Supplementary Tables.

Highlights

- *In situ* imaging coupled with deep learning resolved distributions of plankton in the Northern California Current Ecosystem.
- Artificial intelligence accurately classified plankton images into 161 unique classes.
- *In situ* imagery revealed plankton fine-scale spatial patterns along a historical 57-km transect.

Declaration of interests

☒ The authors declare that they have no known competing financial interests or personal relationships that could have appeared to influence the work reported in this paper.

☐The authors declare the following financial interests/personal relationships which may be considered as potential competing interests: